HHS Public Access

Author manuscript

Retina. Author manuscript; available in PMC 2017 December 01.

Published in final edited form as:

Retina. 2016 December ; 36(Suppl 1): S118–S126. doi:10.1097/IAE.0000000000001328.

Toward quantitative OCT angiography: visualizing blood flow speeds in ocular pathology using variable interscan time analysis (VISTA)

Stefan B. Ploner, BSc[1,2], **Eric M. Moult, BSc**[1], **WooJhon Choi, PhD**[1], **Nadia K. Waheed, MD MPH**[3,*], **ByungKun Lee, MEng**[1], **Eduardo A. Novais, MD**[3,4], **Emily D. Cole, BSc**[3], **Benjamin Potsaid, PhD**[1,5], **Lennart Husvogt, BSc**[2], **Julia Schottenhamml, BSc**[1,2], **Andreas Maier, PhD**[2], **Philip J. Rosenfeld, MD PhD**[6], **Jay S. Duker, MD**[3], **Joachim Hornegger, PhD**[2,7], and **James G. Fujimoto, PhD**[1]

[1]Department of Electrical Engineering and Computer Science, Research Laboratory of Electronics, Massachusetts Institute of Technology, Cambridge, MA

[2]Pattern Recognition Lab., Friedrich-Alexander University Erlangen-Nürnberg (FAU), Erlangen, Germany

[3]New England Eye Center, Tufts Medical Center, Boston, Massachusetts

[4]Federal University of São Paulo, School of Medicine, São Paulo, Brazil

[5]Praevium Research Inc., Santa Barbara, California

[6]Department of Ophthalmology, Bascom Palmer Eye Institute, University of Miami Miller School of Medicine, Miami, Florida

[7]Erlangen Graduate School in Advanced Optical Technologies (SAOT), Erlangen, Germany

Structured Abstract

PURPOSE—Currently available optical coherence tomography (OCT) angiography (OCTA) systems provide information about blood flux, but limited information about blood flow speed. We develop a method for mapping the previously proposed variable interscan time analysis (VISTA) algorithm into a color display that encodes relative blood flow speed.

METHODS—OCTA was performed with a 1050 nm, 400 kHz A-scan rate, swept source OCT system using a 5 repeated B-scan protocol. VISTA was used to compute the OCTA signal from B-scan pairs having 1.5 ms and 3.0 ms interscan times. The resulting VISTA data were then mapped to a color space for display.

RESULTS—We evaluated the VISTA visualization algorithm in normal eyes (n=2), non-proliferative diabetic retinopathy (NPDR) eyes (n=6), proliferative diabetic retinopathy (PDR) eyes (n=3), geographic atrophy (GA) eyes (n=4), and exudative age-related macular degeneration

[*]**Corresponding Author/Reprint Requests**. Correspondence to Nadia K. Waheed MD MPH, New England Eye Center at Tufts Medical Center, 260 Tremont Street, Biewend Building, 9 - 11th Floor, Boston, MA 02116, T: 617-636-7950 / F: 617-636-4866 / nadiakwaheed@gmail.com.

Conflicts of Interest: There are no conflicting relationships for any other author.

(AMD) eyes (n=2). All eyes showed blood flow speed variations, and all eyes with pathology showed abnormal blood flow speeds compared to controls.

CONCLUSIONS—We developed a novel method for mapping VISTA into a color display, allowing visualization of relative blood flow speeds. The method was found useful, in a small case series, for visualizing blood flow speeds in a variety of ocular diseases, and serves as a step towards quantitative OCTA.

Keywords

Ocular blood flow; variable interscan time analysis (VISTA); optical coherence tomography (OCT); optical coherence tomography angiography (OCTA); age-related macular degeneration (AMD); nascent geographic atrophy (GA); choroidal neovascularization (CNV)

Introduction

A variety of ocular pathologies are caused by, and/or result in, alterations of the retinal and choriocapillaris vasculatures. For example, age-related macular degeneration (AMD) and diabetic retinopathy (DR), both of which are leading causes of blindness and severe vision loss in developed countries,[1–3] are associated with alterations of the retinal and choriocapillaris vasculatures.[4–16] Retinal, and, to a lesser extent, choroidal vasculatures have traditionally been imaged with dye-based methods, namely fluorescein angiography (FA) and indocyanine green angiography (ICGA).[17, 18] More recently, optical coherence tomography (OCT) angiography (OCTA) has emerged as a non-invasive method for volumetrically visualizing retinal and choroidal vasculatures *in vivo*.[19–30] OCTA has its roots in Doppler OCT, a technique that measures the Doppler shifts caused when flowing erythrocytes scatter the OCT beam.[31–39] OCTA uses a repeated B-scan protocol wherein multiple B-scans are acquired from the same tissue location in rapid succession. The principle idea of OCTA is that if a region of tissue is stationary—that is, there is no flowing blood in the region—the repeated B-scans will be identical; however, if the tissue's optical scattering is time-dependent—that is, there is blood flow through the region—the repeated B-scans will differ. By comparing repeated B-scans, for example via decorrelation, information about blood flow can be inferred and microvasculature visualized.

Variable interscan time analysis (VISTA), an OCTA imaging and analysis technique proposed by Choi and Moult et al., was developed to overcome the limitation that typical OCTA does not directly measure blood flow speeds.[40] Although a summary of the technique is outlined herein, interested readers are referred to the previous publication for details. Because OCTA signals are related to blood flux through a non-linear, and generally unknown, statistical distribution, in practice OCTA signals are primarily used to detect the presence or absence of vasculature, rather than to infer blood flow speed information. We can understand that OCTA measures blood flux—that is, the blood volume per unit area per unit time—and not blood flow speed by noting that, in general, OCTA computations are influenced not only by the speed at which the scattering blood constituents travel, but also by their density. In describing the VISTA algorithm, we hypothesized a relationship between blood flux and the OCTA signal. In this relationship there are three essential regions of blood flux. The first, relates to low blood fluxes that cannot be detected by OCTA. The

second relates to blood fluxes that can be both detected and distinguished from one another. Finally, the third relates to blood fluxes that can be detected but cannot be distinguished from one another. Accordingly, to be fully correct, a qualifier must be added to the previous statement: OCTA detects the presence or absence of vessels *whose blood flux is within a certain range*. This qualifier is necessitated by the fact that any OCTA system has a smallest detectable flux, and a largest distinguishable flux. Vessels having blood fluxes smaller than the smallest detectable flux cannot be distinguished from background noise; vessels having blood fluxes larger than the largest distinguishable flux cannot be distinguished from one another. The underlying idea of the VISTA algorithm is to exploit the fact that the smallest detectable flux and largest distinguishable flux are functions of the interscan time.

Although the VISTA algorithm allows for differentiation of blood flow speeds, it has not yet been developed into an easily interpretable, clinically useful form. The current methodology for viewing VISTA is to compare, side-by-side, OCTA images corresponding to different effective interscan time. While such comparison is sufficient for making simple observations, it is, in general, difficult to visualize the differences in the blood flow speeds without close inspection. The aim of this paper is to present a methodology for displaying and interpreting VISTA information in a clear, concise fashion that allows clinicians to visualize relative blood flow speeds. We demonstrate the method's utility by visualizing the choroidal, choriocapillaris, and retinal vasculatures in a small case series of different pathologies.

Methods

Subjects

This study protocol was approved by the Institutional Review Boards at the Massachusetts Institute of Technology (MIT) and Tufts Medical Center. All participants were imaged in the ophthalmology clinic at the New England Eye Center (NEEC) and written informed consent was obtained prior to imaging. The research adhered to the Declaration of Helsinki and the Health Insurance Portability and Accountability Act. All subjects underwent a complete ophthalmic examination including a detailed history, refraction, intraocular pressure measurement, anterior segment examination and a dilated fundus examination by an ophthalmologist at the NEEC.

SS-OCT and SS-OCTA Imaging

OCTA was performed using an ultrahigh speed SSOCT research prototype developed at MIT and in use at NEEC. A similar OCT system was described previously and therefore only key characteristics are summarized herein.[30] The prototype OCT instrument uses a vertical cavity surface emitting laser (VCSEL) swept light source with a 400 kHz A-scan rate. The light source is centered at 1050 nm wavelengths which, when compared to the 840 nm wavelengths used in most commercial systems, enables deeper light penetration into the RPE, choroid, and reduced attenuation from ocular opacities.[41] OCT interferometric signals are acquired with an analog-to-digital acquisition card externally clocked at a maximum frequency of ~1.1 GHz using an external Mach-Zehnder interferometer.

OCTA imaging was performed with 6 mm × 6 mm and 3 mm × 3 mm fields of view. For both field sizes, 5 repeated B-scans from 500 uniformly spaced locations were sequentially acquired. Each B-scan consisted of 500 A-scans and the fundamental interscan time between repeated B-scans was ~1.5 ms, accounting for the mirror scanning duty cycle. The acquisition time for repeated B-scans was ~7.5 ms (~1.5 ms × 5) per position. A total of 5 × 500 × 500 A-scans were acquired per OCTA volume for a total acquisition time of ~3.9 s. The volumetric scan pattern yields isotropic transverse sampling of the retina at 12 μm and 6 μm intervals for the 6 mm × 6 mm and 3 mm × 3 mm field sizes, respectively. Smaller field sizes have proportionately more transverse sample density and provide higher OCTA image quality.

Image Analysis

OCTA images were generated using the VISTA algorithm by calculating a decorrelation signal on a pixel-by-pixel basis between sequential OCT B-scans (1↔2, 2↔3, 3↔4, and 4↔5), and every-other scan (1↔3, 2↔4, 3↔5); the former corresponds to the fundamental interscan time of ~1.5 ms, while the latter corresponds to an effective interscan time of ~3.0 ms. For additional details regarding the VISTA algorithm, interested readers are referred to Choi and Moult et al.[40] To correct for eye motion, which produces spurious decorrelation signals, the repeated B-scans were motion corrected using a rigid registration algorithm prior to calculating decorrelation. For each B-scan location and interscan time, the OCTA images were averaged to improve the signal-to-noise ratio. This was performed at all 500 B-scan locations in order to obtain a three-dimensional OCTA volume. In order to compensate for patient motion, 2 orthogonally oriented volumes were acquired from each eye. These volumes were then registered and merged using a previously described algorithm.[42, 43] From these OCTA volumes we computed projections of the volume over various depths, with the exact depth depending on the particular feature we were interested in studying.

The VISTA data generated were visualized using the method described below. With the OCTA images computed, the process of visualizing the VISTA images can be partitioned into two, primarily parallel, phases (Figure 1). One phase, on the left of Figure 1, computes, for each image pixel, the brightness value of that pixel in the final VISTA display; in our chosen display, the pixel brightness is representative of the blood flux. The other phase, shown on the right of Figure 1, computes, for each image pixel, the hue (color) of the pixel in the final VISTA display; the pixel hue represents the blood flow speed at that pixel. These two stages are detailed below.

The first step in computing the VISTA brightness values is to take, for each pixel, the maximum of the two input OCTA images. It is usually the case that the image formed from the larger effective interscan time—in our case 3 ms—contains the higher decorrelation value; however, due to the stochastic nature of sampling, it can happen that the shorter interscan time—in our case 1.5 ms—actually contains the higher decorrelation value. After the maximum operation, the image contrast is adjusted by remapping the pixel intensities in the 1% and 99% quantiles to the values 0 (black) and 1 (white), to normalize the contrast; the remaining pixel intensities are then linearly mapped between the black and white levels.

In the next step, the cases of retinal and CC vasculatures are handled differently. In the case of OCTA images of the retinal vasculature, a Frangi vesselness filter, which emphasizes vascular features, is applied to the contrast adjusted image.[44] The resulting image is then thresholded and applied to the adjusted brightness image as binary mask, effectively setting pixels between vessels to zero. In doing so, the intercapillary noise, specifically in the hue channel, is significantly reduced. We are able to use a vesselness filter for OCTA images of the retinal vasculature because the vessel structure can be clearly resolved by OCTA. However, this vesselness filter is not applied to choriocapillaris (CC) OCTA images, because the fine vascular CC structure cannot be resolved with the resolution of a typical OCT system.

In the second phase of the algorithm the hue values are determined. First, the pixel-by-pixel ratio of the two input OCTA images is calculated. This ratio is related to the blood flow speed at a given location, as can be seen by considering the VISTA curves presented in Choi and Moult et al.[40] In the next step, a joint bilateral filter is applied to the image to smooth the random fluctuations that are an inevitable consequence of the randomness inherent in blood flow, and the derivative nature of the signal processing used to compute the VISTA image. A joint bilateral filter, rather than a Gaussian, is used to preserve vessel boundaries. In the case of CC images, the weights for the filter are derived from the adjusted maximum OCTA image, while in the case of retinal images, the weights for the filter are derived from the vesselness masked adjusted image. Because the hue value of each VISTA pixel is, in essence, a ratio of the decorrelation value obtained from the 1.5 ms interscan time to the decorrelation value obtained from the 3.0 ms interscan time, the values above unity are likely the result of a high blood flow speed. This motivates setting these ratios to unity, which in our convention corresponds to the fastest displayed blood flow speed. After this adjustment, the VISTA pixels are clamped at pre-defined high and low values, and linearly remapped; the clamping values differ for the retinal and choroidal images, and were chosen empirically in order to maximize the dynamic ranges. The rationale behind choosing different clamping values for the retinal and choroidal images is that the retinal and choroidal vasculatures comprise ocular blood supplies with different characteristics.

In the final step of the algorithm the brightness and hue images are used to display the images in a pseudo-HSV (hue, saturation, value) color space, which was modified to have a more uniform color gradient/distribution. We adopted the convention of showing slower blood flow speeds in blue, and faster blood flow speeds in red.

Results

We evaluated our VISTA visualization algorithm on normal control eyes (n = 2; age = 48.0 ± 7.1) (Figure 2), eyes with non-proliferative diabetic retinopathy (NPDR) (n = 6; age = 56.7 ± 7.3) (Figure 3), eyes with proliferative diabetic retinopathy (PDR) (n = 3; age = 49.4 ± 4.4)(Figure 4), eyes with geographic atrophy (GA) (n = 4; age = 78.2 ± 2.8) (Figure 5), and exudative AMD patients (n = 2; age = 84.5 ± 7.8) (Figure 6). In normal controls we observed a blood flow speed gradient, with higher speeds associated with the larger retinal vasculatures, and slower speeds associated with smaller vessels. In patients with NPDR we observed slower speeds associated with capillary looping, and in PDR patients we observed

slower speeds associated with neovascular lesions. In patients with GA, we observed a distribution of blood flow speeds associated within the choroidal vessels underlying the region of atrophy; we also observed lower blood flow speeds in certain areas beyond the margins of atrophy. In patients with exudative AMD we observed a distribution of speeds associated with the lesions, with faster speeds being associated with the trunk of the lesion, and slower speeds associated with the lesion extremities.

Discussion

The ability to visualize blood flow speed changes—as opposed to simply the presence or absence of blood flux—has the potential to be valuable for studying a variety of ocular diseases, particularly those whose pathogenesis proceeds through different stages of flow impairment, rather than an immediate progression to total vascular atrophy. The previously proposed VISTA algorithm provides a way to extend OCTA in order to infer information about relative blood flow speeds; however, its clinical utility was limited by lack of an effective method of viewing the VISTA data. The algorithm presented here addresses this limitation, and maps the raw VISTA data into an easily interpretable color space.

The relative blood flow speeds visualized by our VISTA algorithm are consistent with those that would be expected based on physical principles and prior literature.[45] In particular, in the normal control eyes we observed a gradient of blood flow speeds, with faster speeds being associated with the larger retinal vessels, and slower speeds being associated with the smaller retinal vessels. We also observed slower blood flow speeds associated with capillary looping and neovascularization. We suspect that the slower blood flow speeds in these cases are related to the tortuosity and vessel caliber; here, our findings are difficult to place in the context of prior studies because, to our knowledge, there have been no studies investigating local blood flow speeds in these lesions.

In this study we performed VISTA using two different interscan times—1.5 ms, and 3.0 ms. However, it should be noted that VISTA is extendable to an arbitrary number of interscan times. In general, as more interscan times are added, a finer gradation of blood flow speeds is appreciable. There are, however, a number of caveats. First, as the effective interscan time increases, the likelihood of patient motion accumulating between repeated B-scans also increases, which can have a deleterious effect on image quality. Addressing this limitation requires use of accurate motion correction methods, through hardware based eye tracking, computational post-processing, or a combination thereof. The second issue, which is a result of speed at which ocular blood flows, is that as the interscan time becomes longer, the probability of sampling in the third region of blood, as described in the Introduction, increases. The third region of blood flow, characterized by blood flows that can be detected but not distinguished from one another, does not provide additional information when sampled multiple times. Accordingly, as the number of interscan times increases, we would likely need to reduce the fundamental interscan time. Reducing the fundamental interscan time also has the advantage of allowing higher speed blood flows to be resolved, such as those that may occur in larger vasculature. Reducing the fundamental interscan time requires improved galvanometer scanning performance and, if the same fields and sampling densities

are desired, increased A-scan rates. Despite these challenges, we believe that generalizing VISTA to multiple (> 2) interscan times is a promising direction of future research.

When interpreting the results of this study, as well as the capabilities of the presented algorithm, there are a number of important limitations to consider. First, the number of analyzed eyes was small, meaning that the observations made in this study may not generalize to larger cohorts. Second, it is important to stress that the algorithm presented provides a scheme to visualize *relative* blood flow speeds, not *absolute* blood flow speeds. Furthermore, while our observed results were consistent with previous literature, we did not validate our algorithm explicitly, for example, by using a flow phantom. While such validation studies would be interesting, they are themselves limited, as it is difficult to faithfully mimic *in vivo* conditions.

In this paper we have presented a novel method for visualizing relative blood flow speeds, *in vivo*, using OCTA and the VISTA algorithm. Due to the importance that ocular blood flow has in a variety of diseases, we expect that this method will be useful for studying the pathogenesis of ocular disease. Furthermore, these current efforts are a first step towards developing fully quantitative OCTA technology, which would prove invaluable in not only studying ocular disease, but also in developing endpoints for therapeutic trials.

Acknowledgments

Financial Support: This work was in part supported by a grant from the Macula Vision Research Foundation, New York, National Institute of Health (NIH R01-EY011289-29A, R44-EY022864, R01-CA075289-16, FA9550-15-1-0473 and FA9550-12-1-0499). EAN is a researcher supported by CAPES Foundation, Ministry of Education of Brazil, Brasilia, DF, Brazil.

Jay S. Duker is a consultant for and receives research support from Carl Zeiss Meditec and OptoVue. Nadia K. Waheed was a consultant for Iconic therapeutics, served the speaker's bureau for Thrombogenics, and received research support from Carl Zeiss Meditec, Inc. Philip J. Rosenfeld has received research funding and speaker fees from Carl Zeiss Meditec. Joachim Hornegger: Royalties from property owned by Massachusetts Institute of Technology and licensed to Optovue. James G. Fujimoto: Royalties from intellectual property owned by the Massachusetts Institute of Technology and licensed to Carl Zeiss Meditec Inc., Optovue Inc.; Stock options – Optovue Inc.

References

1. Engelgau MM, Geiss LS, Saaddine JB, et al. The Evolving Diabetes Burden in the United States. Annals of Internal Medicine. 2004; 140:945–950. [PubMed: 15172919]
2. Thylefors B, Négrel AD, Pararajasegaram R, et al. Global data on blindness. Bulletin of the World Health Organization. 1995; 73:115–121. [PubMed: 7704921]
3. Thylefors B. A GLOBAL INITIATIVE FOR THE ELIMINATION OF AVOIDABLE BLINDNESS. Community Eye Health. 1998; 11:1–3. [PubMed: 17492014]
4. Sarks JP, Sarks SH, Killingsworth MC. Evolution of geographic atrophy of the retinal pigment epithelium. Eye. 1988; 2:552–577. [PubMed: 2476333]
5. McLeod DS, Grebe R, Bhutto I, et al. Relationship between RPE and Choriocapillaris in Age-Related Macular Degeneration. Investigative Ophthalmology & Visual Science. 2009; 50:4982–4991. [PubMed: 19357355]
6. Mullins RF, Johnson MN, Faidley EA, et al. Choriocapillaris Vascular Dropout Related to Density of Drusen in Human Eyes with Early Age-Related Macular Degeneration. Investigative Ophthalmology & Visual Science. 2011; 52:1606–1612. [PubMed: 21398287]

7. Bhutto I, Lutty G. Understanding age-related macular degeneration (AMD): Relationships between the photoreceptor/retinal pigment epithelium/Bruch's membrane/choriocapillaris complex. Molecular Aspects of Medicine. 2012; 33:295–317. [PubMed: 22542780]
8. Biesemeier A, Taubitz T, Julien S, et al. Choriocapillaris breakdown precedes retinal degeneration in age-related macular degeneration. Neurobiology of Aging. 2014; 35:2562–2573. [PubMed: 24925811]
9. Mullins, RF.; Khanna, A.; Schoo, DP., et al. Is Age-Related Macular Degeneration a Microvascular Disease?. In: Ash, JD.; Grimm, C.; Hollyfield, JG., et al., editors. Retinal Degenerative Diseases. Vol. 801. New York: Springer; 2014. p. 283-289.
10. McLeod DS, Taomoto M, Otsuji T, et al. Quantifying Changes in RPE and Choroidal Vasculature in Eyes with Age-Related Macular Degeneration. Investigative Ophthalmology & Visual Science. 2002; 43:1986–1993. [PubMed: 12037009]
11. Cogan DG, Toussaint D, Kuwabara T. Retinal vascular patterns: Iv. diabetic retinopathy. Archives of Ophthalmology. 1961; 66:366–378. [PubMed: 13694291]
12. Toussaint DD, Dustin PP. ELectron microscopy of normal and diabetic retinal capillaries. Archives of Ophthalmology. 1963; 70:96–108. [PubMed: 13993857]
13. Klein R, Meuer SM, Moss SE, et al. REtinal microaneurysm counts and 10-year progression of diabetic retinopathy. Archives of Ophthalmology. 1995; 113:1386–1391. [PubMed: 7487599]
14. Sjølie AK, Klein R, Porta M, et al. Retinal microaneurysm count predicts progression and regression of diabetic retinopathy. Post-hoc results from the DIRECT Programme. Diabetic Medicine. 2011; 28:345–351. [PubMed: 21309844]
15. Bresnick GH, Condit R, Syrjala S, et al. ABnormalities of the foveal avascular zone in diabetic retinopathy. Archives of Ophthalmology. 1984; 102:1286–1293. [PubMed: 6477244]
16. Cao J, McLeod D, Merges CA, et al. CHoriocapillaris degeneration and related pathologic changes in human diabetic eyes. Archives of Ophthalmology. 1998; 116:589–597. [PubMed: 9596494]
17. Bischoff P, Flower R. Ten years experience with choroidal angiography using indocyanine green dye: a new routine examination or an epilogue? Documenta Ophthalmologica. 1985; 60:235–291. [PubMed: 2414083]
18. Flower RW. Extraction of choriocapillaris hemodynamic data from ICG fluorescence angiograms. Investigative Ophthalmology & Visual Science. 1993; 34:2720–2729. [PubMed: 8344794]
19. Makita S, Hong Y, Yamanari M, et al. Optical coherence angiography. Optics Express. 2006; 14:7821–7840. [PubMed: 19529151]
20. Fingler J, Schwartz D, Yang C, et al. Mobility and transverse flow visualization using phase variance contrast with spectral domain optical coherence tomography. Optics Express. 2007; 15:12636–12653. [PubMed: 19550532]
21. Mariampillai A, Standish BA, Moriyama EH, et al. Speckle variance detection of microvasculature using swept-source optical coherence tomography. Optics Letters. 2008; 33:1530–1532. [PubMed: 18594688]
22. Jia Y, Tan O, Tokayer J, et al. Split-spectrum amplitude-decorrelation angiography with optical coherence tomography. Optics Express. 2012; 20:4710–4725. [PubMed: 22418228]
23. Huang Y, Zhang Q, Thorell MR, et al. Swept-source OCT Angiography of the Retinal Vasculature using Intensity Differentiation Based OMAG Algorithms. Ophthalmic surgery, lasers & imaging retina. 2014; 45:382–389.
24. Kurokawa K, Sasaki K, Makita S, et al. Three-dimensional retinal and choroidal capillary imaging by power Doppler optical coherence angiography with adaptive optics. Optics Express. 2012; 20:22796–22812. [PubMed: 23037430]
25. Braaf B, Vienola KV, Sheehy CK, et al. Real-time eye motion correction in phase-resolved OCT angiography with tracking SLO. Biomedical Optics Express. 2013; 4:51–65. [PubMed: 23304647]
26. Schwartz DM, Fingler J, Kim DY, et al. Phase-Contrast Optical Coherence Tomography: A New Technique for Non-Invasive Angiography. Ophthalmology. 2014; 121:180–187. [PubMed: 24156929]
27. Kim DY, Fingler J, Zawadzki RJ, et al. Optical imaging of the chorioretinal vasculature in the living human eye. Proceedings of the National Academy of Sciences. 2013; 110:14354–14359.

28. Choi W, Mohler KJ, Potsaid B, et al. Choriocapillaris and Choroidal Microvasculature Imaging with Ultrahigh Speed OCT Angiography. PLoS ONE. 2013; 8:e81499. [PubMed: 24349078]
29. Kim DY, Fingler J, Zawadzki RJ, et al. Noninvasive Imaging of the Foveal Avascular Zone with High-Speed, Phase-Variance Optical Coherence Tomography. Investigative Ophthalmology & Visual Science. 2012; 53:85–92. [PubMed: 22125275]
30. Choi W, Potsaid B, Jayaraman V, et al. Phase-sensitive swept-source optical coherence tomography imaging of the human retina with a vertical cavity surface-emitting laser light source. Optics Letters. 2013; 38:338–340. [PubMed: 23381430]
31. White BR, Pierce MC, Nassif N, et al. In vivo dynamic human retinal blood flow imaging using ultra-high-speed spectral domain optical Doppler tomography. Optics Express. 2003; 11:3490–3497. [PubMed: 19471483]
32. Izatt JA, Kulkarni MD, Yazdanfar S, et al. In vivo bidirectional color Doppler flow imaging of picoliter blood volumes using optical coherence tomography. Optics Letters. 1997; 22:1439–1441. [PubMed: 18188263]
33. Leitgeb RA, Schmetterer L, Hitzenberger CK, et al. Real-time measurement of in vitro flow by Fourier-domain color Doppler optical coherence tomography. Optics Letters. 2004; 29:171–173. [PubMed: 14744000]
34. Wang Y, Bower BA, Izatt JA, et al. In vivo total retinal blood flow measurement by Fourier domain Doppler optical coherence tomography. Journal of Biomedical Optics. 2007; 12:041215–041218. [PubMed: 17867804]
35. Makita S, Fabritius T, Yasuno Y. Quantitative retinal-blood flow measurement with three-dimensional vessel geometry determination using ultrahigh-resolution Doppler optical coherence angiography. Optics Letters. 2008; 33:836–838. [PubMed: 18414549]
36. Wang Y, Lu A, Gil-Flamer J, et al. Measurement of total blood flow in the normal human retina using Doppler Fourier-domain optical coherence tomography. The British journal of ophthalmology. 2009; 93:634–637. [PubMed: 19168468]
37. Baumann B, Potsaid B, Kraus MF, et al. Total retinal blood flow measurement with ultrahigh speed swept source/Fourier domain OCT. Biomedical Optics Express. 2011; 2:1539–1552. [PubMed: 21698017]
38. Schmoll T, Kolbitsch C, Leitgeb RA. Ultra-high-speed volumetric tomography of human retinal blood flow. Optics Express. 2009; 17:4166–4176. [PubMed: 19259253]
39. Choi W, Baumann B, Liu JJ, et al. Measurement of pulsatile total blood flow in the human and rat retina with ultrahigh speed spectral/Fourier domain OCT. Biomedical Optics Express. 2012; 3:1047–1061. [PubMed: 22567595]
40. Choi W, Moult EM, Waheed NK, et al. Ultrahigh-Speed, Swept-Source Optical Coherence Tomography Angiography in Nonexudative Age-Related Macular Degeneration with Geographic Atrophy. Ophthalmology. 2015; 122:2532–2544. [PubMed: 26481819]
41. Unterhuber A, Považay B, Hermann B, et al. In vivo retinal optical coherence tomography at 1040 nm-enhanced penetration into the choroid. Optics Express. 2005; 13:3252–3258. [PubMed: 19495226]
42. Kraus MF, Liu JJ, Schottenhamml J, et al. Quantitative 3D-OCT motion correction with tilt and illumination correction, robust similarity measure and regularization. Biomedical Optics Express. 2014; 5:2591–2613. [PubMed: 25136488]
43. Kraus MF, Potsaid B, Mayer MA, et al. Motion correction in optical coherence tomography volumes on a per A-scan basis using orthogonal scan patterns. Biomedical Optics Express. 2012; 3:1182–1199. [PubMed: 22741067]
44. Frangi, AF.; Niessen, WJ.; Vincken, KL., et al. Multiscale vessel enhancement filtering. In: Wells, WM.; Colchester, A.; Delp, S., editors. Medical Image Computing and Computer-Assisted Intervention — MICCAI'98: First International Conference Cambridge, MA, USA, October 11–13, 1998 Proceedings; Springer Berlin Heidelberg; Berlin, Heidelberg. 1998. p. 130-137.
45. Riva CE, Grunwald JE, Sinclair SH, et al. Blood velocity and volumetric flow rate in human retinal vessels. Investigative Ophthalmology & Visual Science. 1985; 26:1124–1132. [PubMed: 4019103]

Summary Statement

We develop a methodology for visualizing blood flow speeds in ocular pathology using OCTA and VISTA.

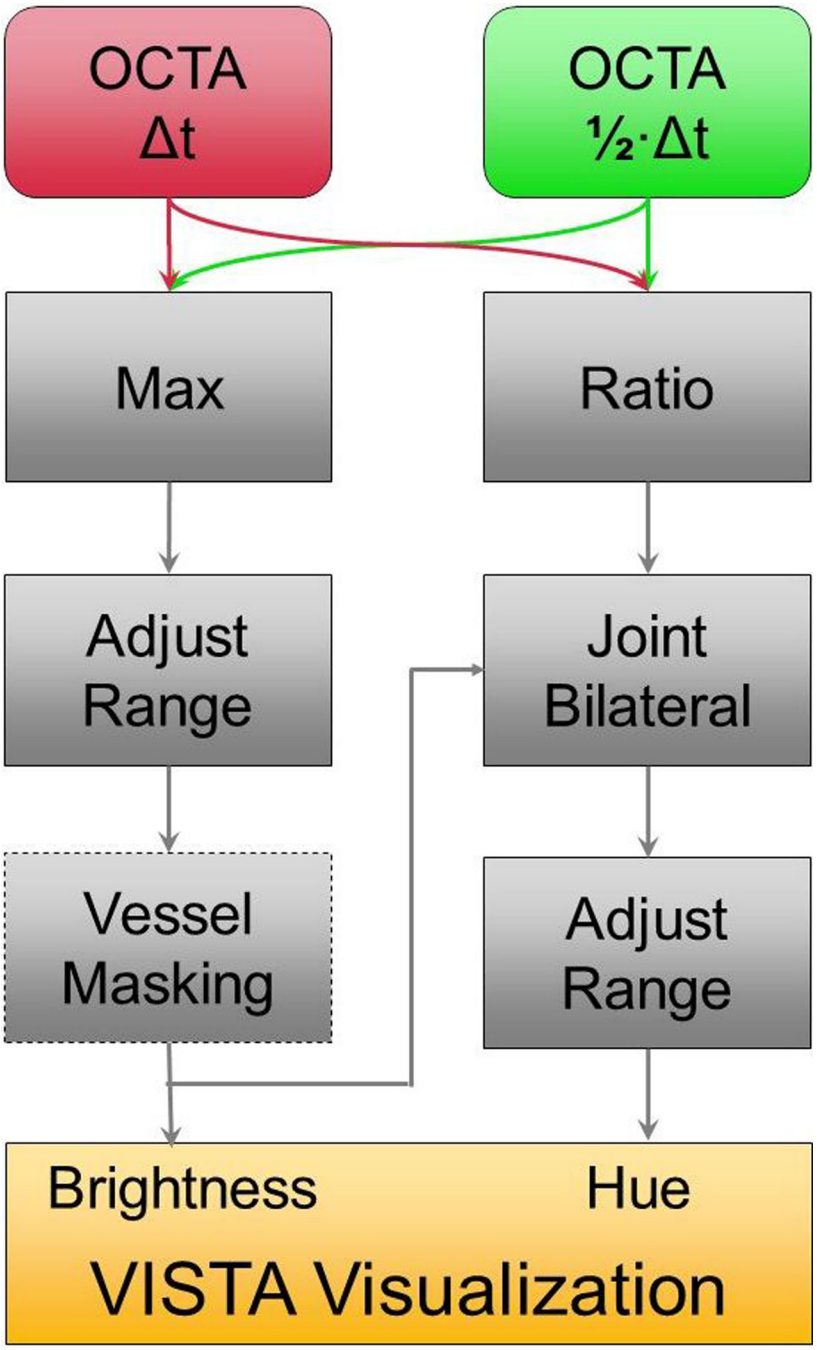

Figure 1.

Workflow of the VISTA visualization algorithm. The inputs to the algorithm are the two distinct interscan time OCTA projections. The algorithm proceeds in two, essentially parallel, phases. One phase, depicted on the left of the figure, computes the brightness values of the VISTA image; the other phase, depicted on the right of the figure, computes the hue (color) of the VISTA image. This brightness and hue data is then displayed, forming the final VISTA image. For projections of the retinal vasculature, a vessel masking filter (dashed

box) is used to suppress intercapillary hue artifacts; in CC OCTA, this filter cannot be used because the vascular structure of the CC is below the optical resolution of our OCT system.

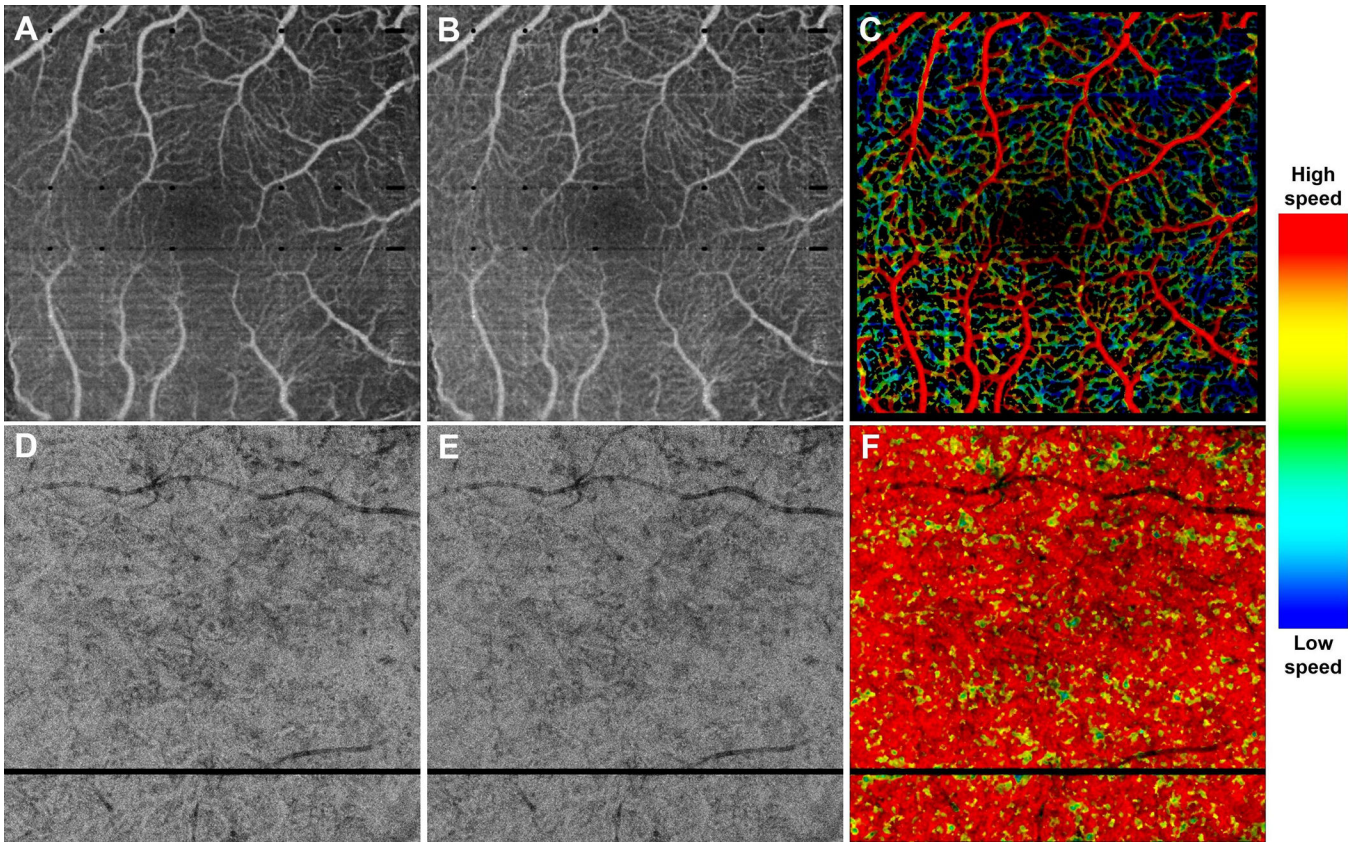

Figure 2.

VISTA visualization in a 43 year old normal patient, taken over (A–C) a 3 mm × 3 mm field of view, and (D–F) a 6 mm × 6 mm field of view. (A) Mean projection of the 1.5 ms OCTA volume through the depths spanned by the retinal vasculature. (B) Mean projection of the 3.0 ms OCTA volume through the depths spanned by the retinal vasculature. (C) VISTA image; red indicates faster blood flow speeds, blue slower speed. Note the blood flow speed gradient, with the larger retinal vessels associated with faster speeds, and the smaller retinal vessels associated with slower speeds. (D) Mean projection of the 1.5 ms OCTA volume through ~90 um slab, lying below the Bruch's membrane. (E) Mean projection of the 3.0 ms OCTA volume through ~90 um slab, lying below the Bruch's membrane. (F) VISTA image; red indicates faster blood flow speeds, blue slower speeds. Note the homogenous speed in the CC vasculature. The color bar on the right side indicates the relation between color and blood flow speed. The same color bar is used for all VISTA color images in this paper.

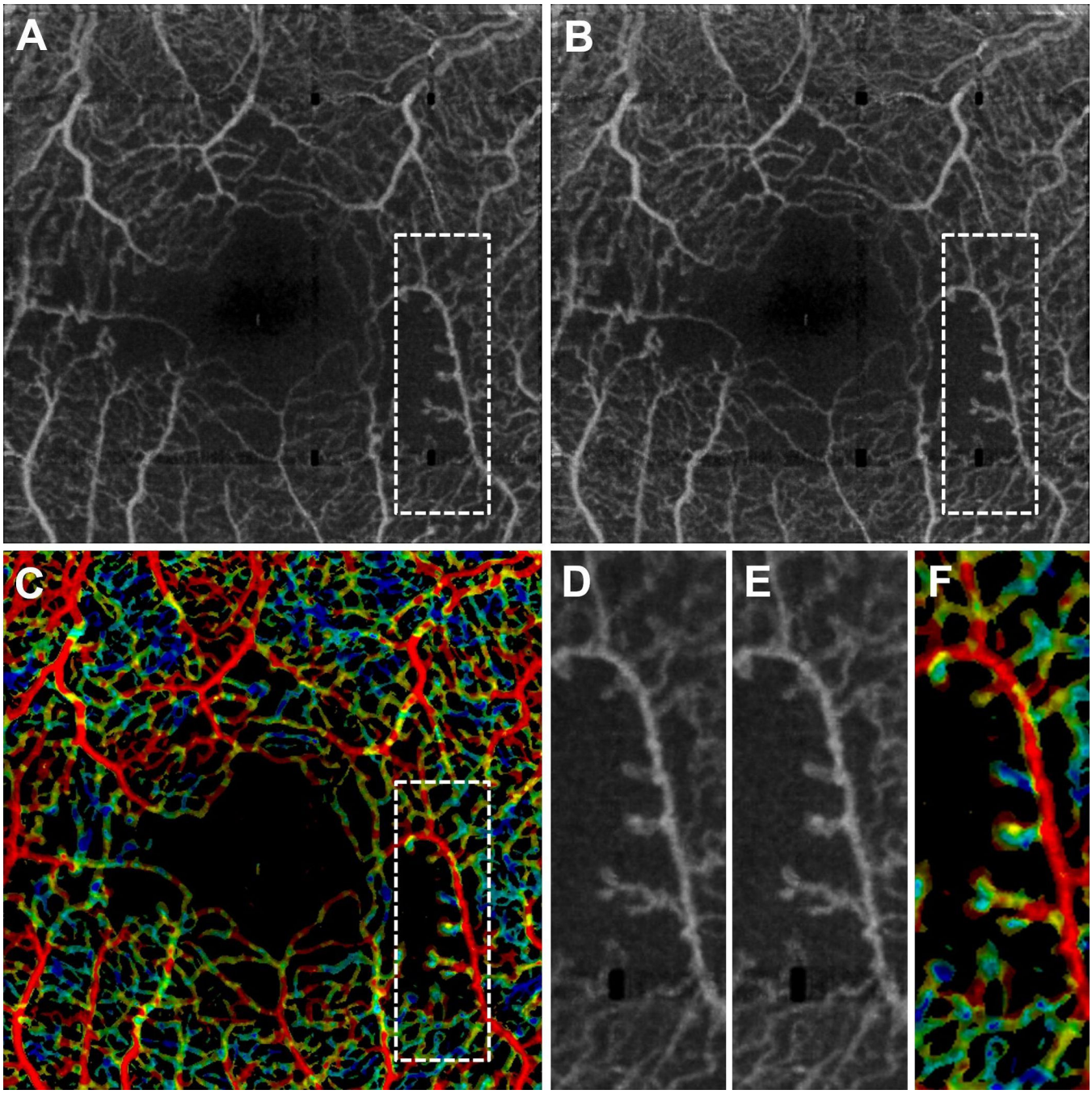

Figure 3.

VISTA visualization in a 53 year old NPDR patient taken over a 3 mm × 3 mm field of view. (A) Mean projection of the 1.5 ms OCTA volume through the depths spanned by the retinal vasculature. (B) Mean projection of the 3.0 ms OCTA volume through the depths spanned by the retinal vasculature. (C) VISTA image; red indicates faster blood flow speeds, blue slower speeds. (D), (E), and (F), are enlargements of the dashed boxes in (A), (B), and (C), respectively. Notice that the capillary loops, which likely correspond to microaneurysms, are associated with slower blood flow speeds.

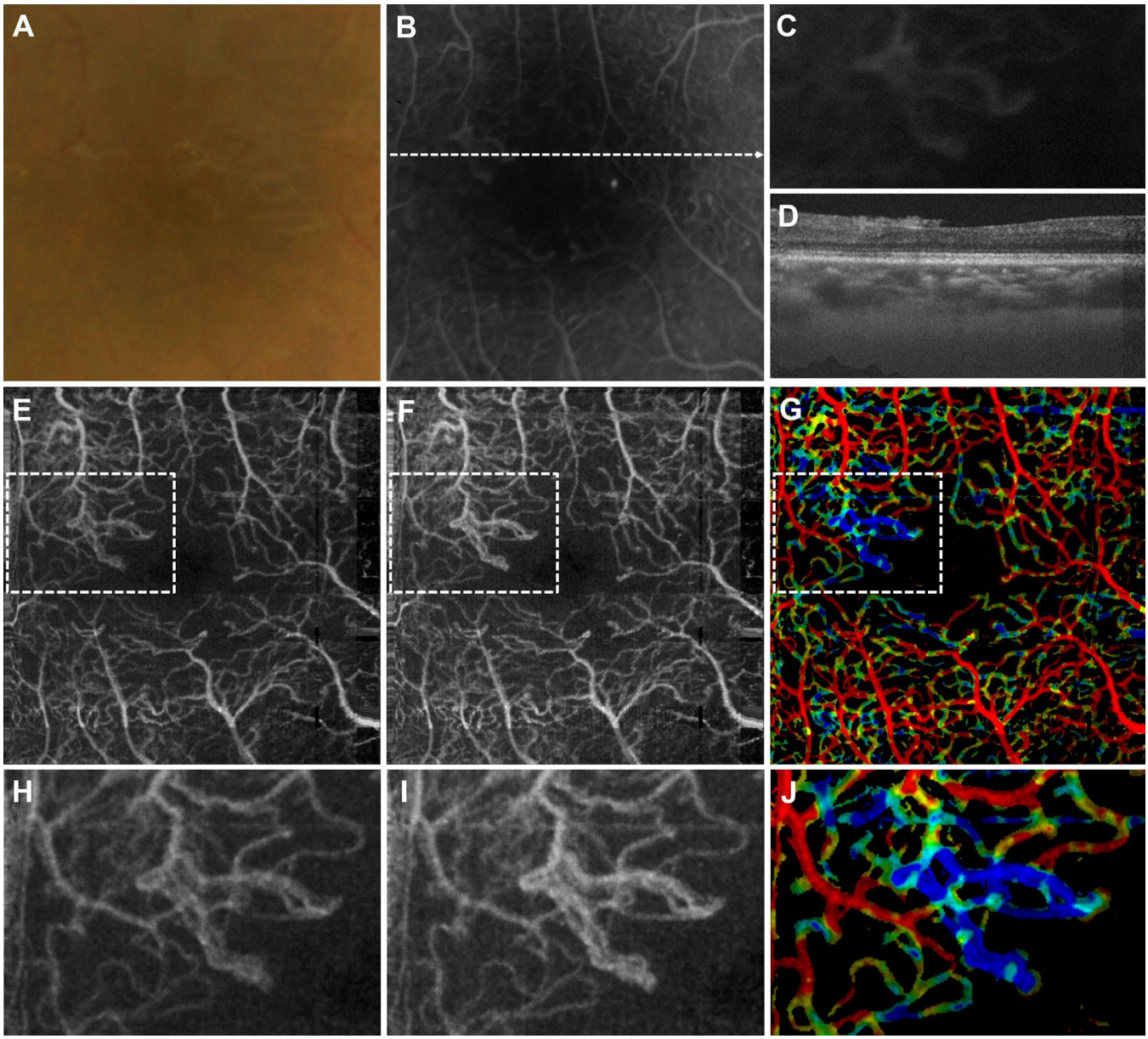

Figure 4.

VISTA visualization in a 30 year old PDR patient taken over a 3 mm × 3 mm field of view. (A) Fundus photo, cropped over the OCT field of view. (B) FA, cropped over the OCT field of view. (C) Enlargement of the FA image about the neovascular lesion. (D) OCT B-scan taken through the dashed line in (B). The neovascular lesion is seen lying above the retina. (E) Mean projection of the 1.5 ms OCTA volume through the depths spanned by the retinal vasculature. (F) Mean projection of the 3.0 ms OCTA volume through the depths spanned by the retinal vasculature. (G) VISTA image; red indicates faster blood flow speeds, blue slower speeds. (H), (I), and (J) are enlargements of the dashed boxes in (E), (F), and (G), centered on the neovascular lesion. Notice how the lesion is associated with slower blood flow speeds.

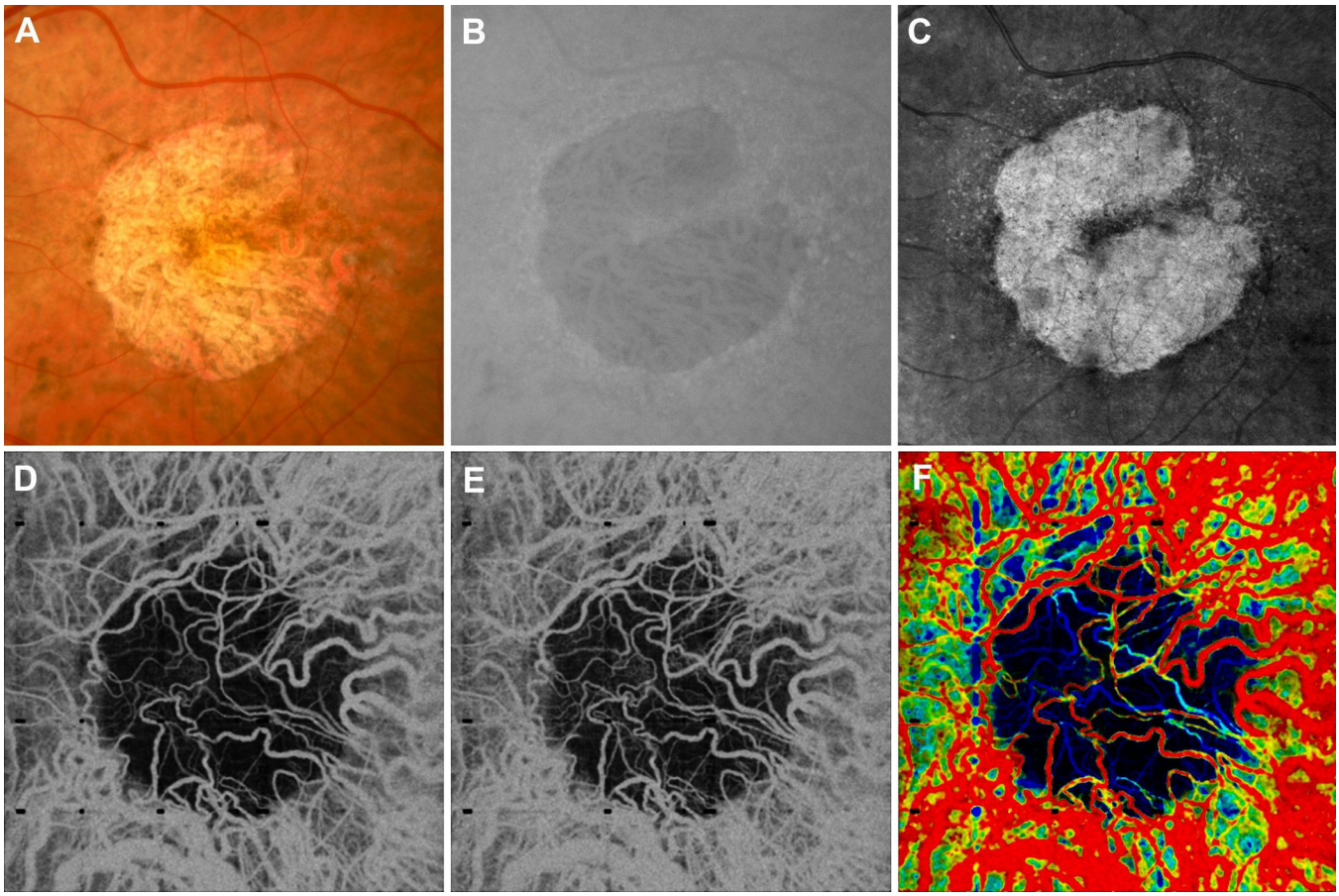

Figure 5.

VISTA in a 75 year old GA patient taken over a 6 mm × 6 mm field of view. (A) Fundus photo, cropped over the OCT field of view. (B) FAF, cropped over the OCT field of view. (C) Mean *en face* projection of the entire OCT volume. (D) Mean projection of the 1.5 ms OCTA volume through ~90 um slab, lying below the Bruch's membrane. (E) Mean projection of the 3.0 ms OCTA volume through ~90 um slab, lying below the Bruch's membrane. (F) VISTA image; red indicates faster blood flow speeds, blue slower speeds. Note that the OCT volume was not flattened and therefore, due to the curvature of the retina, the ~90 um slab, while lying roughly near where the Bruch's membrane would be located near the center of the field of view, intersects deeper choroidal vasculature on the edges of the image. Note that the readily visible choroidal vessels in the region of atrophy show a distribution of blood flow speeds. Also note that on the left of the margin of the VISTA image, appearing green, there is an area of relatively slow blood flow speed. This is indicative of CC flow impairment on the GA margin.

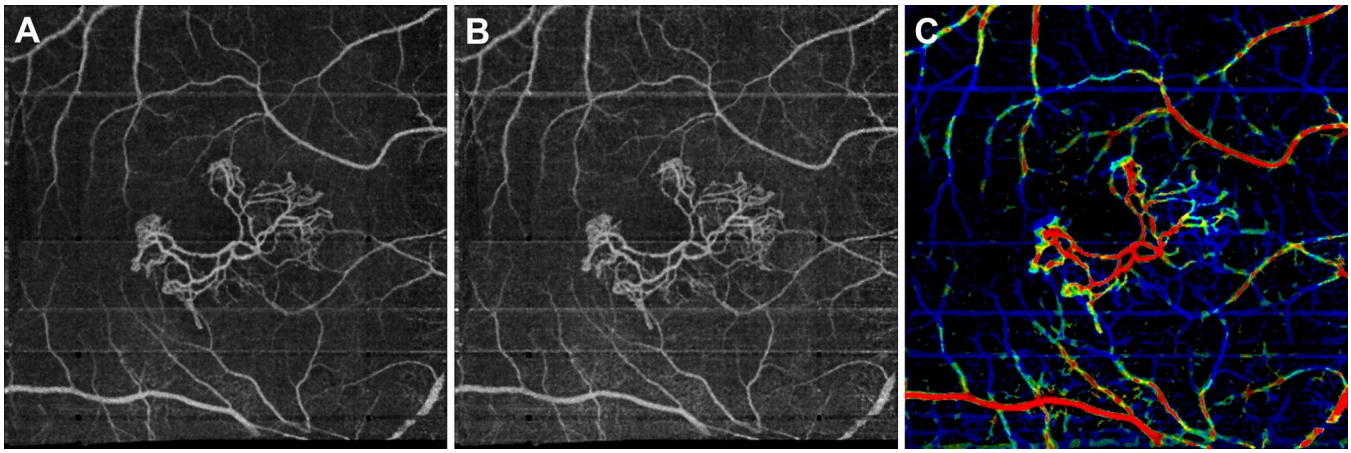

Figure 6.

VISTA visualization in a 90 year old exudative AMD patient, with a treated choroidal neovascular (CNV) lesion, taken over a 6 mm × 6 mm field of view. (A) Mean projection of the 1.5 ms OCTA volume through the depths spanned by the lesion. (B) Mean projection of the 3.0 ms OCTA volume through the depths spanned by the lesion. (C) VISTA image; red indicates faster blood flow speeds, blue slower speeds. Note how the neovascular lesion exhibits a range of blood flow speeds, with faster speeds associated with the trunk of the lesion, and slower speeds associated with its extremities. Note that retinal vessels generate decorrelation tails in the image.